Melanocortin-3 receptor regulates the normal fasting response

Benjamin J. Renquist[a,1], Jonathan G. Murphy[b], Emily A. Larson[c], Dawn Olsen[c,d], Robert F. Klein[c,d], Kate L. J. Ellacott[a], and Roger D. Cone[a,2]

[a]Department of Molecular Physiology and Biophysics, Vanderbilt University School of Medicine, Nashville, TN 37232; [b]Department of Pharmacology, University of Colorado Denver School of Medicine, Aurora, CO 80045; [c]Bone and Mineral Unit, Department of Medicine, Oregon Health and Science University, Portland, OR 97201; and [d]Portland Veterans Affairs Medical Center, Portland, OR 97201

Edited by Stephen O'Rahilly, University of Cambridge, Cambridge, United Kingdom, and approved April 5, 2012 (received for review February 4, 2012)

The melanocortin-3 receptor–deficient (MC3-R$^{-/-}$) mouse exhibits mild obesity without hyperphagia or hypometabolism. MC3-R deletion is reported to increase adiposity, reduce lean mass and white adipose tissue inflammation, and increase sensitivity to salt-induced hypertension. We show here that the MC3-R$^{-/-}$ mouse exhibits defective fasting-induced white adipose tissue lipolysis, fasting-induced liver triglyceride accumulation, fasting-induced refeeding, and fasting-induced regulation of the adipostatic and hypothalamic-adrenal-pituitary axes. Close examination of the hypothalamic-pituitary-adrenal axis showed that MC3-R$^{-/-}$ mice exhibit elevated nadir corticosterone as well as a blunted fasting-induced activation of the axis. The previously described phenotypes of this animal and the reduced bone density reported here parallel those of Cushing syndrome. Thus, MC3-R is required for communicating nutritional status to both central and peripheral tissues involved in nutrient partitioning, and this defect explains much of the metabolic phenotype in the model.

energy homeostasis | nonesterified fatty acid | corticotrophin-releasing hormone | hormone-sensitive lipase

Research on the central melanocortin system has focused on the role of the melanocortin-4 receptor (MC4-R) in energy homeostasis, particularly as a result of the hyperphagic obesity syndrome found in both mice and humans with mutations in this receptor (1–3). A large body of work has demonstrated that circuitry regulated by the MC4-R is essential for much of leptin action and coordinates energy intake with energy expenditure to maintain long-term energy homeostasis (4). In contrast, the melanocortin-3 receptor (MC3-R), expressed in ∼35 different nuclei in the CNS with a pattern distinct from that of the MC4-R (5), has not yet been associated definitively with a human obesity syndrome (6), and the mild obesity syndrome in the MC3-R$^{-/-}$ mouse has not yet been explained mechanistically.

In situ hybridization demonstrated the highest expression of MC3-R mRNA in the arcuate nucleus, ventromedial hypothalamus, medial habenula, ventral tegmental area, and raphe nucleus (5). Not surprisingly, MC3-R mRNA is found primarily in areas of the brain that receive direct innervation from proopiomelanocortin (POMC)-immunoreactive neurons. However, MC3-R also is located on POMC-expressing neurons in the arcuate nucleus (7), where the receptor may function as an inhibitory autoreceptor on melanocortin signaling (8).

The obesity syndrome in the MC3-R$^{-/-}$ mouse is unusual, particularly compared with diet-induced obese (DIO) and MC4-R$^{-/-}$ obesity models, which demonstrate hyperphagia, increased lean mass, increased adipose mass across all depots, hyperlipidemia, hyperinsulinemia, hepatic steatosis, and inflammation in white adipose tissue (WAT) (9, 10). Lipogenic enzyme mRNA levels, such as that encoding fatty acid synthase, are increased in MC4-R$^{-/-}$ and DIO mice (11) and after treatment of WT mice with the dual MC3-R/MC4-R antagonist, SHU9119 (12) but not in the MC3-R$^{-/-}$ mouse (11). In contrast, deletion of the MC3-R produces an obesity syndrome with a loss in lean mass and increase in adipose mass (13, 14). Remarkably, although MC3-R deletion does not impact changes in feeding or energy expenditure in response to a high-fat diet (13–15), feeding MC3-R–null mice a high-fat diet results in a percentage of body fat similar to that observed in the hyperphagic MC4-R$^{-/-}$ fed a high-fat diet (40–45%). Despite this gross obesity, MC3-R$^{-/-}$ mice are comparatively resistant to high-fat diet–induced insulin resistance, hepatic steatosis, and inflammation of WAT (11, 15, 16). Thus, in our first characterization of the MC3-R$^{-/-}$ mouse, we described this mouse as a metabolic model of obesity, without the behavioral hyperphagia seen in the MC4-R–null mice (13). The double MC3-R/MC4-R$^{-/-}$ mice are 27% heavier than the MC4-R$^{-/-}$mice, also suggesting independent mechanisms for MC3-R$^{-/-}$– and MC4-R$^{-/-}$–induced obesity (14).

In addition to both positive and negative effects on energy balance, a variety of other physiological effects have been reported for the MC3-R. The MC3-R$^{-/-}$ mouse is resistant to the induction of natriuresis by γ-MSH, is sensitive to hypertension induced by a high-salt diet, and displays defects in circadian rhythms (17, 18). During the course of our studies on obesity in the MC3-R$^{-/-}$ mouse, we found that, although lipogenesis appeared normal, fasting-induced mobilization of fatty acids from adipose tissue was blunted. This observation led to the more detailed analysis of the fasting response, hypothalamic-pituitary-adrenal (HPA) axis, and nutrient partitioning presented here.

Results

MC3-R$^{-/-}$ Mice Lack Fasting-Induced Nonesterified Fatty Acid Release and Hepatic Triacylglycerol Accumulation. Because no increase in lipogenic gene expression was observed in the MC3-R$^{-/-}$ mouse (11), we sought to determine if differences in lipolysis might explain the increased adiposity. When fasted, WT mice display a rise in serum nonesterified fatty acids (NEFAs) as energy is mobilized from adipose tissue (Fig. 1*A*; $P < 0.001$). In contrast, a 16-h fast does not increase serum NEFAs in the MC3-R$^{-/-}$ mouse ($P = 0.99$). Although fasting-induced changes in serum glycerol were not significant, the profiles did follow a pattern similar to that seen with serum NEFAs (Fig. 1*B*). In culture the release of fatty acids from adipose tissue explants harvested from fed or fasted animals mirrored serum NEFA concentrations, confirming that a decrease in the release of fatty acids from adipose tissue was responsible for the

Author contributions: B.J.R., R.F.K., K.L.J.E., and R.D.C. designed research; B.J.R., J.G.M., E.A.L., D.O., R.F.K., and K.L.J.E. performed research; B.J.R., R.F.K., K.L.J.E., and R.D.C. analyzed data; and B.J.R. and R.D.C. wrote the paper.

The authors declare no conflict of interest.

This article is a PNAS Direct Submission.

[1]Present address: Department of Animal Science, University of Arizona, Tucson, AZ 85718.

[2]To whom correspondence should be addressed: E-mail: roger.cone@vanderbilt.edu.

See Author Summary on page 8808 (volume 109, number 23).

This article contains supporting information online at www.pnas.org/lookup/suppl/doi:10.1073/pnas.1201994109/-/DCSupplemental.

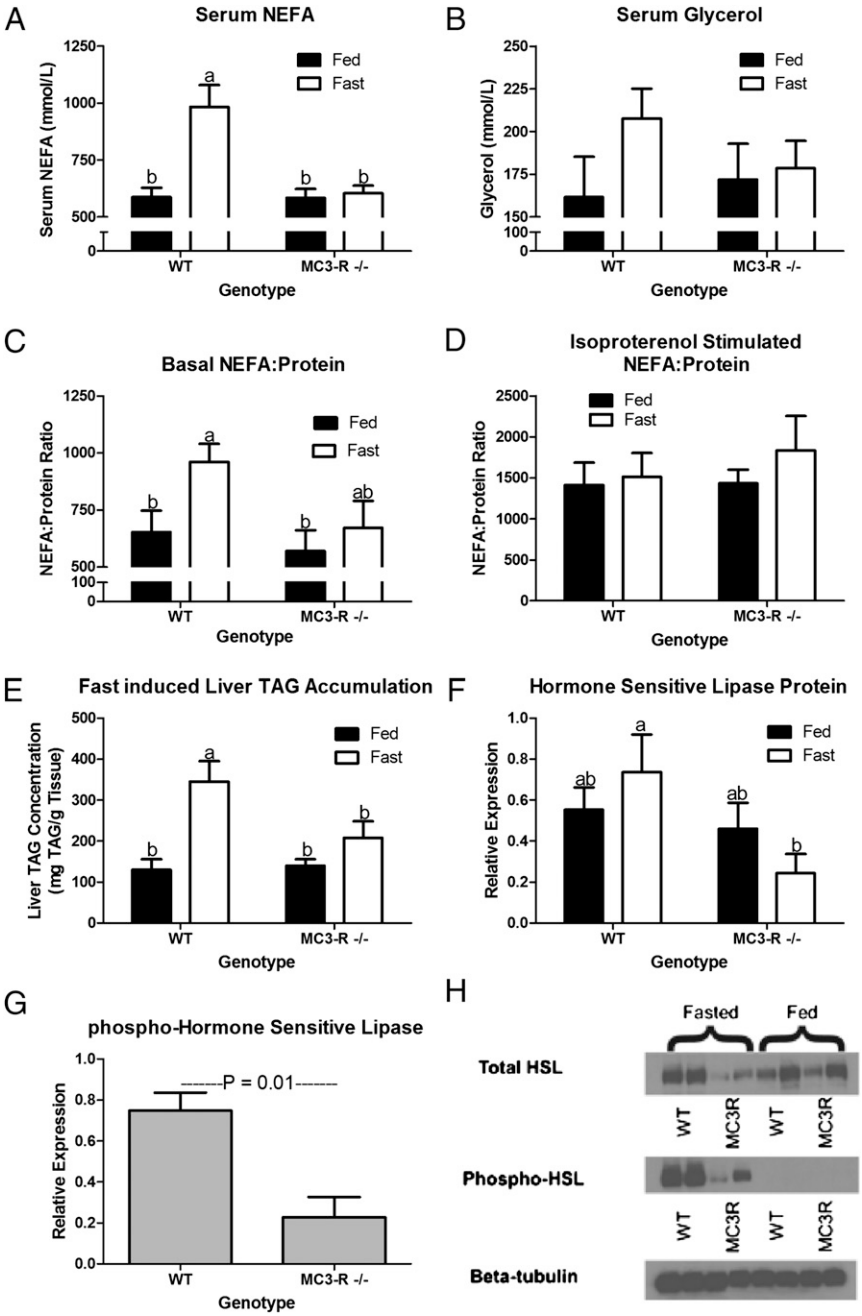

Fig. 1. MC3-R deletion blunts the fasting-induced rise in circulating NEFAs by decreasing their mobilization from adipose tissue. Data in each panel were collected from 12- to 14-wk-old fed (black bars) and 16-h fasted (open bars) WT and MC3-R$^{-/-}$ male mice. (*A*) Serum NEFAs (n = 9–10). (*B*) Serum glycerol (n = 9–10). (*C*) Relative concentration of NEFAs (mmol·L^{-1}·mg^{-1} protein) in medium after 1-h ex vivo incubation of adipose tissue explant at 37 °C in basal medium (n = 10–12). (*D*) Relative concentration of NEFAs (mmol·L^{-1}·mg^{-1} protein) in medium after 1-h ex vivo incubation of adipose tissue explant at 37 °C in 10 μM isoproterenol medium (n = 10–12). (*E*) Fasting-induced liver TAG concentration (n = 7). (*F*) Quantitation of Western blots in *H*. Relative adipose tissue expression of total HSL protein (n = 4). (*G*) Quantitation of Western blots in *H*. Relative phospho-HSL protein expression (n = 4). No measurable phospho-HSL expression was detected in fed mice of either genotype. (*H*) Representative Western blots. Data are expressed as mean ± SE. Bars that do not share a letter (^{a,b}) differ significantly ($P < 0.05$).

blunted fasting-induced rise in serum NEFA in the MC3-R$^{-/-}$ mice (Fig. 1*C*; $P > 0.05$). Capacity for adipose tissue lipolysis was equivalent in fed and fasted WT and MC3-R$^{-/-}$ mice, because explants stimulated with 10 μM isoproterenol released similar amounts of NEFAs (Fig. 1*D*). The rise in serum NEFAs associated with fasting results in the accumulation of triacylglycerol (TAG) in the liver during a fast. As expected, fasting increased TAG concentration in the liver in WT mice, whereas in MC3-R$^{-/-}$ mice, coordinate with a lack of fasting-induced serum NEFAs, there was no rise in liver TAG concentration (Fig. 1*E*). Evaluation of hormone-sensitive lipase (HSL) within adipose tissue showed that total HSL protein was similar in fed WT and MC3-R$^{-/-}$ mice (Fig. 1*F*). However, in the fasted state both total and phosphorylated HSL protein were lower in MC3-R$^{-/-}$ mice than in WT mice (Fig. 1 *F* and *G*; $P < 0.05$ and $P = 0.01$, respectively). Fig. 1*H* shows a representative Western blot of the data quantified in Fig. 1 *F* and *G*.

A fasting-induced decrease in serum glucose was observed in both WT and MC3-R$^{-/-}$ mice but reached significance only in WT mice (Fig. 2*A*). In the fasted state the liver releases glucose derived from glycogenolysis and gluconeogenesis. Liver glycogen decreased significantly in both WT and MC3-R$^{-/-}$ mice, not differing between genotypes in either fed or fasted mice (Fig. 2*B*). Hepatic mRNA for two gluconeogenic enzymes, phosphoenolpyruvate carboxykinase (PEPCK), and glycerokinase increased with fasting in both WT and MC3-R$^{-/-}$ mice (Fig. 2 *C* and *D*). Surprisingly, despite an increase in glycerokinase mRNA, glycerokinase activity did not increase significantly in fasted MC3-R$^{-/-}$ mice (Fig. 2*E*). Perhaps glycerol release from adipose tissue affects glycerokinase activity posttranscriptionally. Despite a robust disturbance in fasting fatty acid metabolism, there is little evidence that MC3-R deletion affects hepatic glucose production. In the absence of elevated glycerol for glucose production, amino acids from skeletal muscle may serve as a substrate for glucose synthesis. The use of amino acids to maintain blood glucose provides a mechanism for the decrease in lean body mass described previously (13, 14).

MC3-R$^{-/-}$ Mice Exhibit Elevated Basal Corticosterone and Defective Fasting-Induced HPA Axis Activation. After observing the defective lipolytic response to a fast, we sought to determine if there was a generalized defect in the stress response in MC3-R$^{-/-}$ mice. First, basal circulating corticosterone was assessed in the MC3-R$^{-/-}$ mouse before total body weight (BW) diverged from WT controls (Table S1). MC3-R deficiency was found to produce a mild hypercorticosteronemia (Fig. 3*A*; $P = 0.02$). Cushing syndrome is characterized by an elevation of cortisol at the daily nadir, and thus the corticosterone circadian pattern was evaluated in samples collected at zeitgeber times 4, 10, 18, and 22. Circadian corticosterone measurements confirmed that MC3-R deletion elevated circulating corticosterone specifically during the daily nadir but not throughout the remainder of the circadian cycle (Fig. 3*B*).

Because MC3-R deletion prevented a fasting-induced rise in NEFAs, we also evaluated the stress responsiveness of the HPA axis to fasting and other stressors. Although fasting increased serum corticosterone nearly sixfold in WT mice, it had no effect in MC3-R$^{-/-}$ mice ($P = 0.99$; Fig. 3*C*). mRNA expression of whole hypothalamic corticotrophin-releasing hormone (CRH) was not different in ad libitum-fed MC3-R$^{-/-}$ or WT mice (Fig. 3*D*). However, the dysregulation in the fasting-induced rise in corticosterone is paralleled by a defect in fasting-induced upregulation of hypothalamic CRH mRNA in the MC3-R$^{-/-}$ mouse (Fig. 3*D*). The lack of a rise in corticosterone in response to a fast was specific to this nutritional stress, because the response to a meal-entrainment stressor or to restraint stress was independent of MC3-R status (Fig. 3 *E* and *F*).

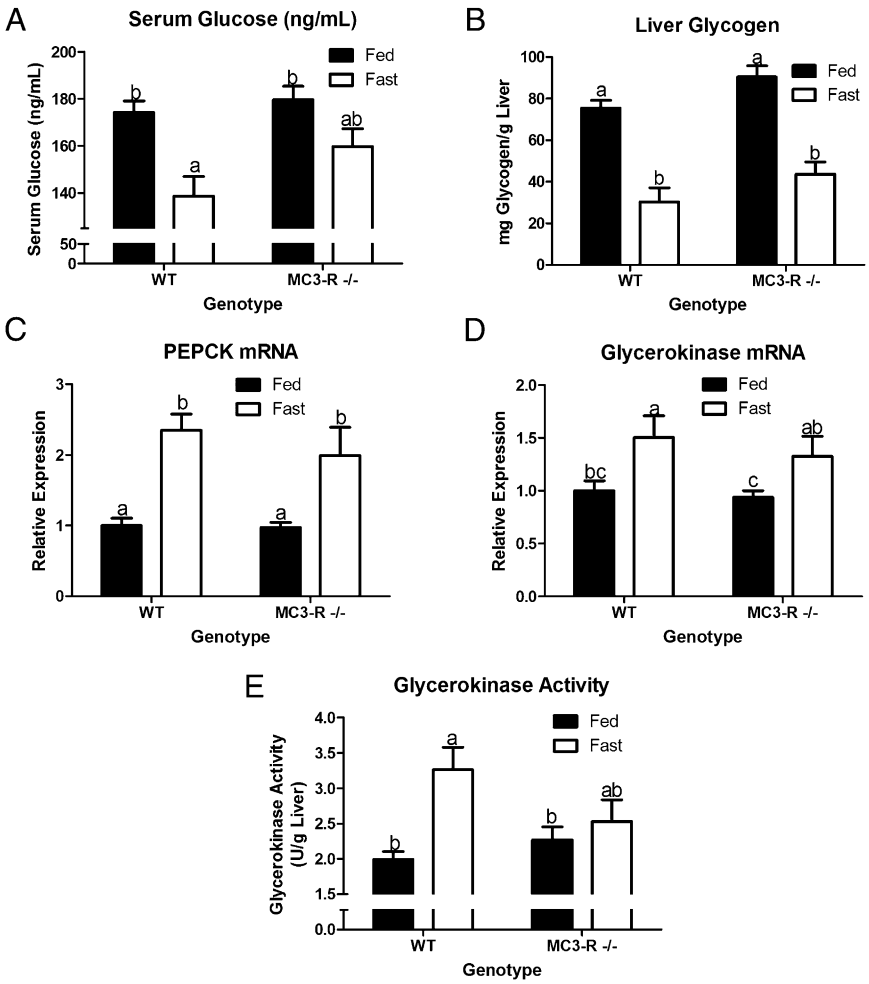

Fig. 2. MC3-R deficiency does not largely affect glucose homeostasis in 12- to 14-wk-old fed (black bars) and 16-h fasted (open bars) WT and MC3-R$^{-/-}$ male mice. (*A*) Serum glucose (n = 9–11). (*B*) Liver glycogen (n = 10–12). (*C*) Liver PEPCK mRNA (n = 7–8). (*D*) Liver glycerokinase mRNA (n = 7–8). (*E*) Liver glycerokinase activity (n = 7–8). Data are expressed as mean ± SE. Bars that do not share a letter (^{a,b,c}) differ significantly ($P < 0.05$).

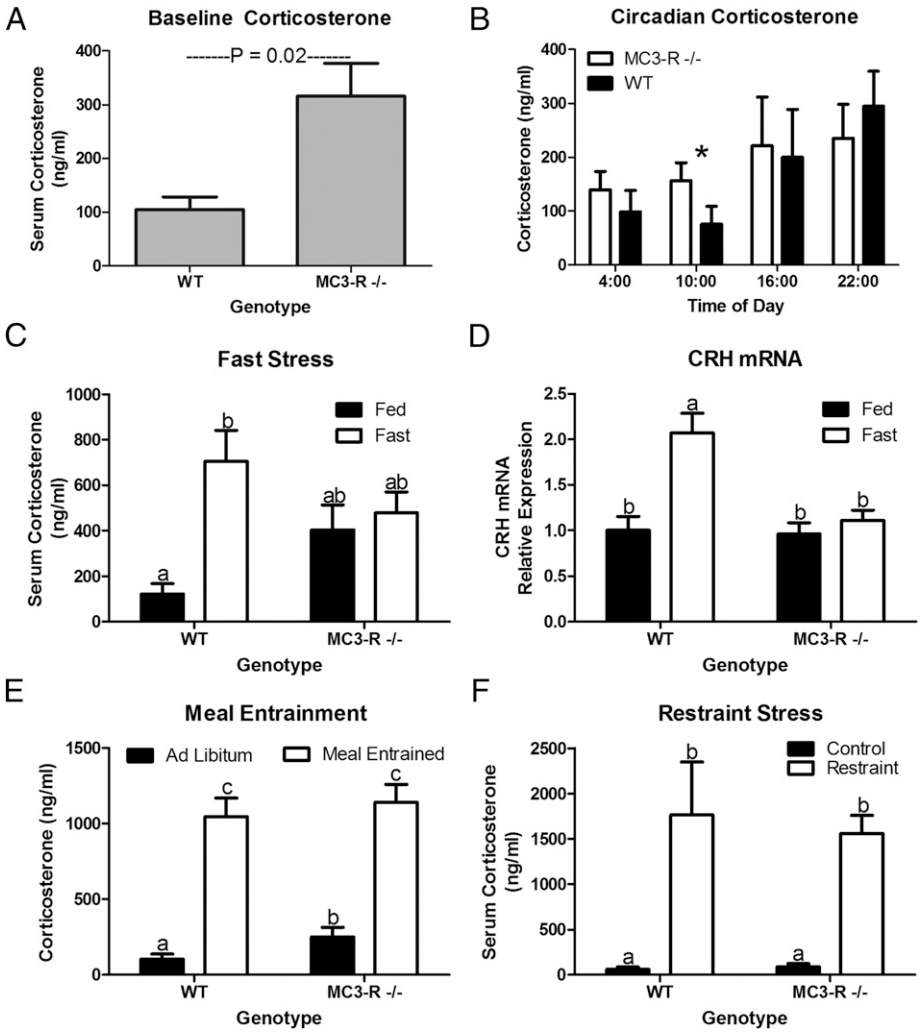

Fig. 3. MC3-R deficiency results in hypercorticosteronemia and stress-specific defects in HPA axis activation. (*A*) Basal serum corticosterone concentrations from 12- to 14-wk-old WT and MC3-R$^{-/-}$ male mice (10:00 AM; n = 17–18). (*B*) Circadian pattern of serum corticosterone concentration shows an elevation in MC3-R$^{-/-}$ mice (open bars) relative to WT mice (black bars) only during the circadian nadir (10:00; *$P < 0.05$, n = 11–15). (*C*) Serum corticosterone concentration in fed (black bars) and 16-h fasted (open bars) 12-wk-old WT and MC3-R$^{-/-}$ male mice (n = 12–14). (*D*) Relative expression of hypothalamic CRH mRNA in fed (black bars) and 16-h fasted (open bars) 12-wk-old WT and MC3-R$^{-/-}$ male mice (n = 9–12). (*E*) Serum corticosterone in ad libitum fed (black bars) (n = 4) and meal-entrained (open bars) (n = 13) WT and MC3-R$^{-/-}$ mice. (*F*) Serum corticosterone 30 min after conclusion of a 5-min restraint stress (open bars) (n = 10). Data are expressed as mean ± SE. Bars that do not share a letter (^{a,b,c}) differ significantly ($P < 0.05$).

Pituitary and Adrenal Physiology in MC3-R$^{-/-}$ Mice. Hypercorticosteronemia frequently is associated with pituitary and adrenal tumors (19), but no visible tumors were found in either pituitary or adrenal glands of 10-mo-old WT or MC3-R$^{-/-}$ mice, and basal serum ACTH levels did not differ. Furthermore, adrenal mass (Fig. 4*A*) and percentage of cortical area (Fig. 4*B*) did not differ in 10-mo-old WT and MC3-R$^{-/-}$ mice. Because MC3-R also is expressed in the adrenal gland, we hypothesized that deletion of MC3-R could affect adrenal ACTH sensitivity directly (20). We tested adrenal response to ACTH in vivo and ex vivo in an explant culture model. ACTH-induced corticosterone release did not differ in WT and MC3-R$^{-/-}$ mice (Fig. 4 *C* and *D*). Analysis of adrenal mRNA from fed WT and MC3-R$^{-/-}$ mice confirmed that there was no genotype difference in baseline expression of melanocortin-2 receptor (MC2-R) mRNA. However, the fasting-induced rise in MC2-R mRNA expression observed in WT mice was absent in fasted MC3-R$^{-/-}$ mice (Fig. 4*E*). Furthermore, fasting-induced increases in the expression of the MC2-R accessory protein (MRAP) and Agouti-related peptide (AgRP) mRNA were absent in MC3-R$^{-/-}$ mice (Fig. 5 *F* and *G*). Thus, basal adrenal function is not affected by MC3-R deletion, but the fasting-induced changes in adrenal physiology are blunted in MC3-R$^{-/-}$ mice.

Defective CNS Responses to Fasting in MC3-R$^{-/-}$ Mice. Because neuropeptide Y (NPY) and AgRP peptides play a role in the fasting-induced increase in CRH mRNA (21, 22), and that the MC3-R$^{-/-}$ mouse displayed a defect in fasting-induced CRH mRNA expression, fasting-induced refeeding and fasting-induced changes in NPY and AgRP mRNA expression were characterized in the MC3-R$^{-/-}$ mouse. Fasting-induced 12-h refeeding was blunted in MC3-R$^{-/-}$ mice (Fig. 5*A*). Furthermore, the fasting-stimulated rise in NPY and AgRP mRNA expression was blunted in the MC3-R$^{-/-}$ mouse (Fig. 5 *B* and *C*). Previous work had suggested that the rise in NPY and AgRP resulted from a local increase in T3 production because of increased expression of deiodinase 2 (DIO2) (23). Fasting-induced up-regulation of DIO2 also is aberrant in the MC3-R$^{-/-}$ mouse (Fig. 5*D*). Thus, the lack of a fasting-induced rise in corticoste-

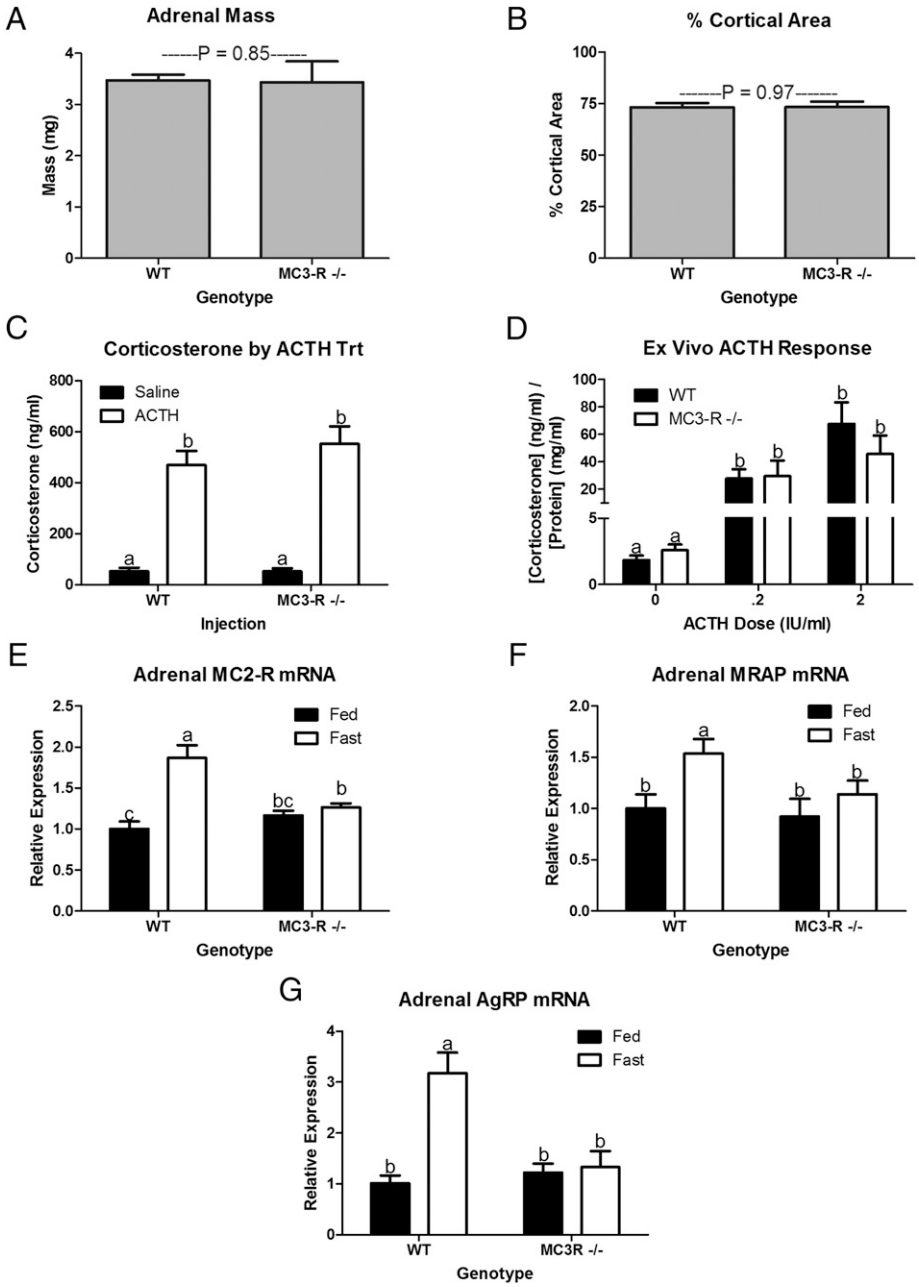

Fig. 4. MC3-R deficiency does not affect adrenal morphology or ACTH responsiveness, but it does blunt the physiological response to fasting. Total adrenal weight (n = 22–26) (*A*) and the percent of cortical area relative to total adrenal area (*B*) did not differ in 12- to14-wk-old WT and MC3-R$^{-/-}$ male mice (n = 5–8). (*C*) In vivo serum corticosterone in response to injection of saline (0.1 mL/10 g BW) (black bars) or ACTH (10 μg/kg BW in 0.1 mL/10 g BW) (open bars) (n = 5–8). (*D*) Ex vivo adrenal corticosterone release in response to 0, 0.2, or 2 IU/mL ACTH. Each well contained two quarters of an adrenal from a single animal in 100 μL medium. Two quartered adrenals from each animal [WT (black bars) (n = 7) and MC3-R$^{-/-}$ (open bars) (n = 5) male mice] were treated with one of the three doses of ACTH. (*E*) Relative MC2-R mRNA expression in fed (black bars) and 16-h fasted (open bars) 12- to14-wk-old WT and MC3-R$^{-/-}$ male mice (n = 9–11). (*F*) Relative adrenal MRAP mRNA expression in fed (black bars) and 16-h fasted (open bars) 12- to 14-wk-old WT and MC3-R$^{-/-}$ male mice (n = 9–11). (*G*) Relative adrenal AgRP mRNA expression in fed (black bars) and 16-h fasted (open bars) 12- to 14-wk-old WT (n = 14 or 15) and MC3-R$^{-/-}$ male mice (n = 10). Data are expressed as mean ± SE. Bars that do not share a letter (^{a,b}) differ significantly ($P < 0.05$).

rone may result from a blunted rise in orexigenic peptides known to induce CRH mRNA expression during a fast.

MC3-R Deletion Results in Phenotypes Common to Cushing Syndrome. MC3-R deletion increased nadir serum corticosterone concentrations (Fig. 3*B*). Previous studies had shown that MC3-R deletion resulted in features common to Cushing syndrome including increased adiposity, decreased lean mass, decreased immune function, and increased sensitivity to salt-induced hypertension (11, 13, 14, 17). Our analyses of adipose tissue distribution and bone mineral density (BMD) and strength confirm two additional phenotypes common to hypercortisolemia.

Hypercorticosteronemia results in increased adiposity with preferential accumulation of visceral adiposity (24). Thus, we expected that the hypercorticosteronemia induced by MC3-R deletion would increase total and percent visceral fat mass. As previously described, deletion of MC3-R increased fat mass ($P < 0.05$) and body fat percentage ($P < 0.001$) without affecting ei-

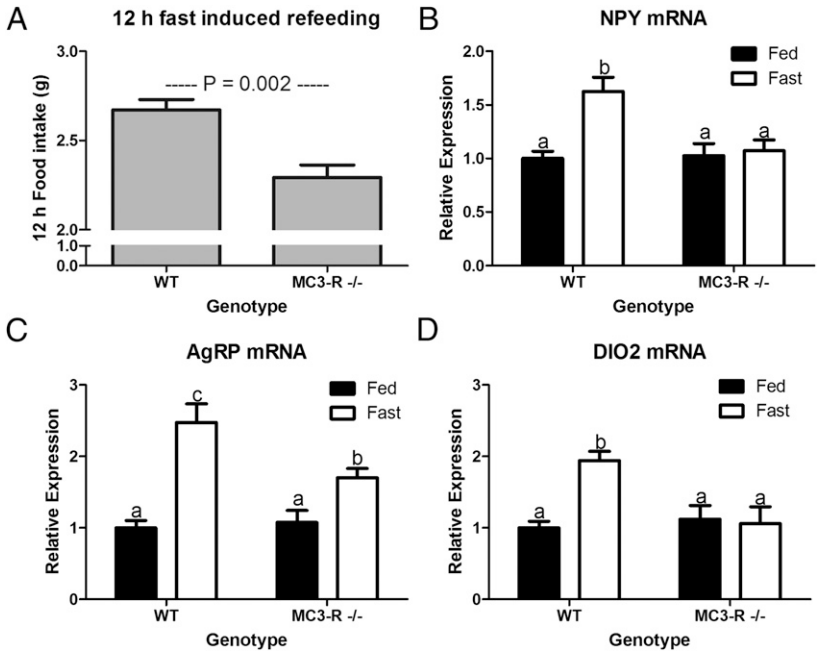

Fig. 5. MC3-R deficiency blunts fasting-induced feeding and up-regulation of orexigenic neuropeptides. (*A*) Twelve-hour food intake following a 16-h fast in 12- to 14-wk-old WT and MC3-R$^{-/-}$ male mice (n = 5). (*B–D*) Relative whole hypothalamic NPY (n = 9–12) (*B*), AgRP (n = 9–12) (*C*), and DIO2 (n = 4–7) (*D*) mRNA expression in fed (black bars) and 16-h fasted (open bars) 12-wk-old WT and MC3-R$^{-/-}$ male mice. Data are expressed as mean ± SE. Bars that do not share a letter (^{a,b}) differ significantly ($P < 0.05$).

ther BW or lean mass (Table S1). Fat pad analysis showed that deletion of MC3-R increased the mass of all depots examined (Fig. S1*A*; $P < 0.05$). However, it was evident that, when expressed in relation to total adipose mass, the increase in adipose tissue mass with MC3-R deletion was specific to two visceral depots (Fig. S1*B*). There was a 10% increase in epididymal adipose tissue mass and a very robust 70% increase in retroperitoneal adipose tissue mass ($P < 0.05$).

MC4-R deletion is known to increase both linear growth (1) and BMD (25, 26), whereas MC3-R deletion was reported previously to decrease linear growth and femur length (14). In light of other Cushing-like phenotypes, and because hypercorticosteronemia is known to favor bone resorption and limit bone deposition, bone properties were analyzed as previously described (27, 28) in 28- to 32-wk-old male MC4-R$^{-/-}$, MC3-R$^{-/-}$, and WT mice. MC4-R deletion increased total whole-body BMD, cancellous area, and polar moment of inertia (I*p*) (Table 1). DIO resulted in very similar increases, and thus the main effects of MC4-R deletion on bone are secondary to obesity. Despite a small increase in total BW at this age, MC3-R$^{-/-}$ mice displayed decreased femur length, BMD, cortical area, and cancellous area relative to WT mice (Table 1). I*p*, a measure of bone strength, decreased 18% with MC3-R deletion ($P < 0.001$). Thus, MC3-R$^{-/-}$ mice display both the increased adiposity and decreased BMD common to elevated corticosterone.

Discussion

The mild obesity syndrome in the MC3-R–knockout mouse has not yet been explained effectively (13, 14). In fact, studies have not demonstrated hyperphagia or hypometabolism in these animals (13, 15, 29), leaving the mechanism of increased adiposity to be determined. In this study, we show a number of specific defects in communication of nutritional status to both the HPA axis and peripheral energy stores that alter nutrient partitioning to increase adiposity. Additionally, we show that MC3-R deletion results in a Cushing-like syndrome with elevated basal corticosterone levels and concomitant effects on adipose tissue distribution and bone remodeling.

Table 1. Physical and mechanical properties of bone in 28- to 32-wk-old male mice

	Study 1*			Study 2†	
Property	WT (n = 13)	MC3-R$^{-/-}$ (n = 10)	MC4-R$^{-/-}$ (n = 7)	WT (n = 8)	DIO (n = 12)
Body weight (g)	26.44 ± 0.49	30.58 ± 1.27**	48.82 ± 1.02***	24.45 ± 0.43	45.32 ± 1.54***
Total bone mineral density (BMD; g/cm^2)	52 ± 0.4	51 ± 0.5*	57 ± 0.6***	51 ± 0.5	54 ± 0.9*
Femur length (mm)	16.07 ± 0.05	15.74 ± 0.08***	16.23 ± 0.05	15.72 ± 0.08	16.07 ± 0.06
Femoral bone mineral density (mg/cm^2)	58.2 ± 1.0	54.0 ± 0.9**	57.9 ± 0.8	53.2 ± 0.6	58.5 ± 1.1**
Cortical area (mm^2)	0.79 ± 0.01	0.74 ± 0.01	0.82 ± 0.02	0.71 ± 0.005	0.82 ± 0.012***
Cancellous area (mm^2)	1.19 ± 0.026	1.08 ± 0.026*	1.34 ± 0.026**	1.04 ± 0.023	1.33 ± 0.040***
I*p* (mm^4)	0.44 ± 0.01	0.36 ± 0.01***	0.50 ± 0.01**	0.35 ± 0.01	0.51 ± 0.016***
Cortical thickness (mm)	0.17 ± 0.002	0.17 ± 0.003	0.17 ± 0.005	0.16 ± 0.002	0.17 ± 0.002*

Data are expressed as mean ± SE. *$P < 0.05$; **$P < 0.01$; ***$P < 0.001$, compared with WT within study by two-tailed t test.
*Study 1: WT, MC3-R$^{-/-}$, and MC4-R$^{-/-}$ mice.
†Study 2: WT and DIO mice.

We report that MC3-R deletion decreases NEFA mobilization from adipose tissue in times of energy deficiency, potentially explaining the increased fat mass despite normophagia and normal energy expenditure. MC3-R$^{-/-}$ mice previously were shown to oxidize less fatty acid than WT mice when fed a low-fat diet but to oxidize similar amounts of fatty acids on a high-fat diet (15). This observation suggests that the MC3-R$^{-/-}$ mouse normally uses fats from the diet but not from endogenous sources. An inability to mobilize NEFAs for energy would result in a change in lean mass, as previously identified in mature MC3-R$^{-/-}$ mice (14). We propose that a lack of HPA axis and CRH neuron activation by low energy stores encountered before normal bouts of feeding may gradually result in this altered body composition.

The CRH neurons are activated by both fasting and feeding and thus are uniquely positioned to affect lipolysis and adipogenesis (30, 31). Paraventricular nucleus (PVN) CRH neurons innervate WAT directly (32, 33). The PVN neurons that send projections to WAT are innervated by POMC neurons from the arcuate nucleus, which express MC3-R, and by NPY neurons in the nucleus of the solitary tract (31). Although we were unable to find any literature on fasting lipolysis rates in visceral adipose tissue from Cushing patients, it is tempting to speculate that a defect in lipolysis explains the increase in visceral adiposity in humans with the disease.

Mouse models that maintain insulin sensitivity despite excess adiposity consistently exhibit either altered fatty acid metabolism or immune response to fatty acids. The adipose triglyceride lipase (ATGL)$^{-/-}$ mouse, PEPCK-overexpressing mouse, and diacylglycerol acyltransferase 1 (DGAT1)-overexpressing mouse all have decreased circulating lipid profiles and are resistant to obesity-induced insulin resistance (34–36). The Toll-like receptor 4 (TLR4) missense mutation mouse and TLR4$^{-/-}$ mouse have altered macrophage activation in response to lipids (37, 38), because fatty acid binding to the TLR4 activates macrophages (38). Together these models suggest that fatty acid release from adipose tissue and subsequent macrophage activation by fatty acids play a role in the development of metabolic syndrome. Therefore, a lack of fasting-induced lipolysis in the MC3-R$^{-/-}$ mouse may explain the reduced insulin resistance and normoglycemia maintained in these animals.

The MC3-R$^{-/-}$ mouse mounts a normal stress response to LPS, restraint stress, and meal entrainment but lacks fasting-induced up-regulation of serum corticosterone (Fig. 3) (39). We conducted studies to determine the origin of this HPA-axis defect. Specifically we examined the fasting response of hypothalamic CRH and adrenal MC2-R, MRAP, and AgRP mRNA. It has been shown previously that hypothalamic CRH increases with a fast (40). We show here that a 16-h fast results in twofold up-regulation in hypothalamic CRH mRNA in the WT mouse that is completely absent in the MC3-R$^{-/-}$ mouse (Fig. 4*B*). Thus, the lack of a corticosterone response to fasting appears to be centrally mediated. Because ACTH up-regulates MC2-R (ACTH receptor) through a cAMP-dependent feed-forward mechanism and because fasting is known to regulate MC2-R expression (41, 42), we monitored the fasting-induced up-regulation of MC2-R. A 16-h fast increased MC2-R mRNA in WT mice but failed to have any effect on MC2-R mRNA expression in MC3-R$^{-/-}$ mice. We also observed a fasting-induced up-regulation of MRAP mRNA in WT mice that did not exist in MC3-R$^{-/-}$ mice. Finally, we monitored AgRP mRNA, because adrenal AgRP expression is up-regulated during a fast and is thought to play a role in controlling corticosterone release (43, 44). Similar to both MC2-R and MRAP, AgRP mRNA was up-regulated by fasting in WT mice but not in MC3-R$^{-/-}$ mice. Thus, both the hypothalamic and adrenal responses to fasting are blunted in the MC3-R$^{-/-}$ mouse.

A previous study demonstrated that CNS-specific deletion of POMC resulted in elevated basal corticosterone levels as well as elevated hypothalamic CRH (45). The data presented here are consistent with this finding and suggest that the MC3-R may mediate this effect. Daily nadir corticosterone levels in the MC3-R$^{-/-}$ mouse are two- to threefold higher than in control littermates. However, corticosterone concentrations during the remainder of the circadian cycle remain normal (Fig. 2*B*). Similarly, some Cushing syndrome patients have elevated nadir and normal peak cortisol concentrations (46). In a previous study that reported normal corticosteronemia in the MC3-R$^{-/-}$ mouse, samples were collected in the afternoon, well after the circadian nadir of corticosterone concentrations (13). The differences in nadir corticosterone were not explained by adrenal mass, cortical area, or adrenal ACTH response.

Additional studies will be required to determine whether deletion of the MC3-R produces a measurable difference in CRH mRNA or peptide levels exclusively in the PVN, because only whole hypothalamic levels were examined in this study. Interestingly, the ventromedial hypothalamus, one of the hypothalamic sites where MC3-R is most abundant (5), also has been implicated in regulation of adrenocortical function (47). Thus, a non–CRH-mediated mechanism leading to elevated basal corticosterone in the MC3-R$^{-/-}$ is possible also. In fact, it is possible that MC3-R deletion from the adrenal gland results in hypercorticosteronemia by eliminating the ability of AgRP to induce its paracrine inhibitory effects on corticosterone (20, 44).

Previous studies from this laboratory and others have published phenotypes in the MC3-R–deficient animal that also are seen in Cushing syndrome. Specifically, MC3-R$^{-/-}$ mice have been shown to exhibit increased adiposity, a deficit in lean mass relative to other obese mouse models, decreased immune function as demonstrated by decreased WAT inflammation, and salt-sensitive hypertension (11, 13, 14, 17). Because reduced bone mass is a classic phenotype of Cushing syndrome, we analyzed bone properties in the MC3-R$^{-/-}$ mouse. However, because of the increased adiposity of MC3-R$^{-/-}$ mice and known effects of adipose-derived hormones in bone remodeling (48, 49), we also analyzed bone phenotypes in two additional obese models, the MC4-R$^{-/-}$ and the DIO mouse. Both diet-induced and genetic obesity increase BMD and bone strength. Despite elevated adiposity and a modest increase in BW, the MC3-R$^{-/-}$ mouse has reduced bone strength, reduced cortical and cancellous area, and reduced I*p* compared with age- and sex-matched WT mice (Table 1). With increased visceral adiposity, decreased lean mass, depressed obesity-associated inflammation, salt-sensitive hypertension, and a decrease in bone mass and strength, it is reasonable to assume that much of the MC3-R$^{-/-}$ phenotype could be explained by elevated nadir corticosterone, as is the case in Cushing syndrome.

However, the previously reported increase in insulin sensitivity despite obesity does not appear to correlate well with the perceived effects of Cushing syndrome on insulin sensitivity. This difference may result from the long-term obesity commonly expressed before a diagnosis of Cushing syndrome. It is possible that Cushing patients also maintain enhanced insulin sensitivity early in their obesity, because the MC3-R$^{-/-}$ mouse does become insulin insensitive after an extended exposure to high-fat diet.

Fasting-induced refeeding was blunted in the MC3-R$^{-/-}$ mouse. Fasting-induced refeeding is also impaired in the NPY$^{-/-}$, DIO2$^{-/-}$, and uncoupling protein 2 (UCP2)$^{-/-}$ mice (23, 50, 51). Interestingly, a single pathway has been proposed to be responsible for the altered fasting-induced refeeding in the NPY-, DIO2-, and UCP2-knockout models. Coppola et al. (23) elegantly describe a pathway whereby arcuate nucleus glial cells convert T4 to T3 via DIO2. T3 induces mitochondrial up-regulation of UCP2 in NPY neurons, thereby increasing their activity and increasing feeding drive. The authors suggest that

the rise in DIO2 is corticosterone dependent. However, we suspect that this rise is corticosterone independent, because adrenalectomy does not prevent fasting-induced up-regulation of NPY and AgRP (52).

Because MC3-R is expressed throughout the arcuate nucleus in both POMC (rostral→caudal; 55–28%) and NPY/AgRP (rostral→caudal; 43–13%) neurons (7), we evaluated this pathway in the MC3-R$^{-/-}$ mouse. We show here that deletion of the MC3-R gene blunts the fasting-induced up-regulation of DIO2, NPY, or AgRP gene expression. We propose that the blunted fasting-induced CRH response results from a blunted NPY and AgRP response. Intracerebroventricular injection of either AgRP or NPY ICV has been shown to increase corticosterone (21, 22). Surprisingly, the MC3/4-R agonist MTII also increases circulating corticosterone (53). Although, initially it appears contradictory for corticosterone to be up-regulated by both anorexigenic and orexigenic neuropeptides, the data parallel the activation of the HPA axis by both fasting and high-fat feeding.

Results from these studies provide a more comprehensive understanding of the obesity syndrome seen in the MC3-R$^{-/-}$ mouse and suggest a specific role for MC3-R–containing circuits in communicating nutritional status to the HPA axis and in appropriately regulating nutrient partitioning from WAT to liver in response to fasting.

Materials and Methods

Animals and Husbandry. All animals used were male MC3-R$^{-/-}$ or WT C57BL6/J mice (13). Mice used in the fasting studies, restraint stress studies, body composition studies, and fat depot analysis studies were 12–14 wk of age. Mice used for the bone density analyses were 28–32 wk of age. MC3-R$^{-/-}$ mice have been crossed onto the C57BL6/J background for more than nine generations. Unless stated otherwise, all animals were housed in three to five to a cage, at 21 ± 2 °C, with ad libitum access to standard chow (Purina rodent diet 5001 or Picolab Mouse Diet 20; Purina Mills) and water. Experiments were conducted in accordance with National Institutes of Health guidelines for the care and use of laboratory animals and were approved by the Animal Care and Use Committees of Oregon Health and Science University and Vanderbilt University.

Sample Collection and Storage. For all studies that ended in mice being killed, animals were anesthetized with halothane or isoflurane using the bell jar method. Once fully anesthetized, mice were killed by decapitation, and trunk blood was collected. Immediately following collection, blood was placed on ice and allowed to clot, and serum was isolated by centrifugation. Serum was stored at −20 °C for analysis of NEFA, glycerol, and glucose using commercially available kits (Wako Diagnostics; Pointe Scientific, Inc.). Serum collected for corticosterone analyses was stored at −80 °C until analyzed using an enzyme immunoassay (EIA) kit (Assay Designs). Whole hypothalamus and liver samples were collected, frozen on dry ice, and stored at −80 °C. Adipose tissue was collected for explant culture as described below.

Fasting Studies. Male MC3-R$^{-/-}$ and WT mice, 12–14 wk of age, were maintained on normal mouse chow (Purina 5001) or fasted overnight (16 h). At 10:00 AM animals were killed.

Restraint Stress Studies. Male MC3-R$^{-/-}$ and WT mice, 12–14 wk old, were placed in 50-mL conical tubes with air holes and were kept restrained for 5 min. Control animals were not handled. At the end of the 5-min restraint animals were returned to their home cages. Thirty minutes after return to the home cage, trunk blood was collected as described previously.

Fast-Refeed Studies. Male MC3-R$^{-/-}$ and WT mice, 12–14 wk of age, were fasted overnight (16 h). At 1000 h animals were provided a weighed amount of food. At 2200 h food was weighed again, and intake was calculated as the difference in food weight from 1000 h to 2200 h.

Adipose Explant Culture. Adipose tissue was collected into tubes containing 0.1 M PBS for analysis of in vitro lipolysis (54). Briefly, visceral WAT was washed several times with 0.1 M PBS. The tissue then was dissected into pieces (15–25 mg) and incubated for 1 h at 37 °C in 250 μL phenol red-free DMEM with 2% (wt/wt) fatty acid-free BSA (Sigma-Aldrich). After 1 h incubation, tissue explants were moved to identical fresh medium for an additional 1-h incubation in the presence or absence of 10 μM isoproterenol (36). Upon completion of the second 1-h incubation, medium was collected and stored at −20 °C until analysis for NEFAs using the commercially available kit previously mentioned. The tissue was washed several times in 0.1 M PBS, placed into a tube containing 300 μL 0.3N NaOH with 0.1% SDS, and sonicated. Because the protein assay is sensitive to lipids, lipids were extracted from the sample by vortexing with an equal volume (300 μL) of 40% trichloroacetic acid and 300 μL of an ice-cold 50:50 mixture of ethanol and diethyl ether. Samples were centrifuged for 10 min at 11,500 × *g*, and supernatant was discarded. After 10 min of drying, the pellet was resuspended in 300 μL 0.3N NaOH with 0.1% SDS for analysis of protein using the bicinchoninic acid (BCA) protein analysis kit (Pierce).

Liver TAG Analysis. Whole liver, collected as described above, was ground using a liquid nitrogen-cooled mortar and pestle. Total liver lipids subsequently were extracted from a sample of the powdered liver using a previously described method (55). Liver lipids were redissolved in a 9:4:2 ratio of t-butanol, Triton X-114, and methanol for analysis using the triglyceride GPO kit (catalog no. T7532; Pointe Scientific).

Total Adrenal and Adrenal Cortex Area. Both adrenal glands were collected in formalin and subsequently were embedded in paraffin for slicing by the Vanderbilt University Medical Center Immunohistochemistry Core Laboratory. Every fifth 5-μM slice was collected on a glass slide. Slides were H&E stained so that adrenal cortex and medulla could be distinguished easily. Pictures were collected at 10× magnification using a Zeiss Imager.Z1 microscope equipped with an AxioCam MRm (Carl Zeiss MicroImaging, Inc). Total adrenal area and cortical area were quantified using Image J software (56). Percent cortical area was calculated using the three images that had the greatest total adrenal area.

ACTH Response. Mice were monitored for in vivo corticosterone response to i.p. injection of ACTH in 0.1 mL saline/10 g BW (10 μg/kg BW) or saline alone. One hour after injection mice were killed by decapitation under isoflurane anesthesia, and trunk blood was collected. Serum was collected after blood was allowed to clot overnight at 4 °C and was spun at 3,000 × *g* for 30 min. Serum corticosterone was measured using an EIA kit (Assay Designs).

To monitor ex vivo ACTH response, we collected both adrenals and quartered them. Two adrenal quarters were put into each of three wells of a 96-well plate with 100 μL of Ringer buffer (pH 7.2) on ice. One hour later medium was changed in all wells, and the quartered adrenals were incubated at 37 °C with 0, 0.02, or 0.2 IU ACTH/100 μL. Media and adrenals were collected. Media were analyzed for corticosterone as described above, and total adrenal protein was analyzed using the BCA assay kit (Thermo Scientific).

Real-Time PCR Analyses. Male MC3-R$^{-/-}$ and WT 12- to 14-wk-old mice were fed or fasted for 16 h (WT, n = 12; MC3-R$^{-/-}$, n = 9) and were killed immediately by cervical dislocation under isoflurane anesthesia. Hypothalamic tissue for analysis of CRH, NPY, POMC, AgRP, and DIO2 and adrenal tissue for analysis of MC2-R, MRAP, and AgRP mRNA expression were collected, frozen immediately on dry ice, and stored at −80 °C. RNA was extracted from the adipose tissue using TRIzol reagent (Invitrogen), followed by cDNA synthesis using the iScript cDNA synthesis kit (Bio-Rad Laboratories) according to the manufacturer's instructions. Taqman gene-expression assays (primer/probe sets) specific to mouse were purchased from Applied Biosystems and run in duplicate on 96-well plates according to the manufacturer's instructions on a Taqman 7300 instrument (Applied Biosystems). Data were adjusted for efficiency of amplification using the LinReg PCR program. Gene expression for each target was normalized to 18S or ACTB mRNA. Samples were adjusted for efficiency

Western Blot. Samples were homogenized in 10 mM Tris·HCL (pH 6.8) with 2% SDS, PhosSTOP phosphatase inhibitor (Roche Diagnostics), and EDTA-free Complete Protease Inhibitor (Roche Diagnostics). Primary antibodies used were rabbit anti-HSL (1:10,000) (Cell Signaling), rabbit anti–phospho (Ser660)-HSL (1:1,000) (Cell Signaling), and mouse anti–β-tubulin (1:2,500) (Developmental Studies Hybridoma Bank, E7 ascites). Secondary antibodies were HRP-conjugated donkey anti-rabbit and donkey anti-mouse (1:2,000) (Jackson ImmunoResearch). Blots were exposed to SuperSignal West Pico Chemiluminescent Substrate (Pierce Biotechnology), and signal was visualized on film. Signal was quantified using ImageJ, and phospho-HSL and HSL expression were normalized to β-tubulin expression (56).

Body Composition Analysis. Whole-animal body composition was assessed in vivo using a dual-energy X-ray absorptiometry (DXA) scanner (PIXImus; GE Healthcare) in 13-wk-old MC3-R$^{-/-}$ and WT mice. The mice were fasted for 16 h to reduce the variability attributed to food in the digestive tract. Immediately before scanning, animals were deeply anesthetized using ketamine/xylazine/acepromazine mouse mixture (0.1 cm^3/g BW), and their BW and nose-to-anus length were measured.

Analysis of Femur Density and Biomechanics. Mice were killed by an overdose of ketamine/xylazine/acepromazine mouse mixture. The left femur from each mouse was excised, wrapped in sterile gauze soaked in 0.1 M PBS, and stored frozen at −20 °C or lower for subsequent analyses.

Whole-femoral BMD was measured by DXA using the PIXImus instrument. The precision for BMD was ±1% for repeat measurements of the same bones. Femoral bone geometry was examined by a desktop X-ray microtomographic scanner (micro-CT) (model 1074; SkyScan). For image acquisition, the specimen was mounted on a turntable to allow 3D imaging with a scan width of 17 μm. Images were stored in 3D arrays and subsequently analyzed with Optimas software (version 6.2; Media Cybernetics,). The CT images were used to compute femoral midshaft cortical bone area (mm^2), cancellous area (mm^2), cortical thickness (mm), and *I*p (mm^4).

Statistical Analysis. All data are reported as raw means and SEs. Bone, fat depot, and body composition data were analyzed using a two-tailed *t* test. All other data were analyzed using mixed model ANOVA in SAS 9.1 (SAS Institute). When no treatment was imposed, the sole independent variable was genotype. When mice were fasted or food restricted, the model included the fixed independent variables genotype, treatment, and their interaction. For variables with replicates, animal was included as a random variable. Differences between least squares means were determined using the pdiff function Bonferroni adjusted for multiple comparisons.

ACKNOWLEDGMENTS. We thank Savannah Y. Williams and Katelijn Van Munster for technical assistance. This work was supported by National Institutes of Health Grant DK078850 (to R.D.C.), and by the VA Medical Research Service and National Institutes of Health Grant R01 AR44659 (to R.F.K.).

1. Huszar D, et al. (1997) Targeted disruption of the melanocortin-4 receptor results in obesity in mice. *Cell* 88:131–141.
2. Vaisse C, Clement K, Guy-Grand B, Froguel P (1998) A frameshift mutation in human MC4R is associated with a dominant form of obesity. *Nat Genet* 20:113–114.
3. Yeo GS, et al. (1998) A frameshift mutation in MC4R associated with dominantly inherited human obesity. *Nat Genet* 20:111–112.
4. Cone RD (2005) Anatomy and regulation of the central melanocortin system. *Nat Neurosci* 8:571–578.
5. Roselli-Rehfuss L, et al. (1993) Identification of a receptor for gamma melanotropin and other proopiomelanocortin peptides in the hypothalamus and limbic system. *Proc Natl Acad Sci USA* 90:8856–8860.
6. Calton MA, et al. (2009) Association of functionally significant Melanocortin-4 but not Melanocortin-3 receptor mutations with severe adult obesity in a large North American case-control study. *Hum Mol Genet* 18:1140–1147.
7. Bagnol D, et al. (1999) Anatomy of an endogenous antagonist: Relationship between Agouti-related protein and proopiomelanocortin in brain. *J Neurosci* 19:RC26.
8. Renquist BJ, Lippert RN, Sebag JA, Ellacott KL, Cone RD (2011) Physiological roles of the melanocortin MC$_3$ receptor. *Eur J Pharmacol* 660:13–20.
9. Bruun JM, Lihn AS, Pedersen SB, Richelsen B (2005) Monocyte chemoattractant protein-1 release is higher in visceral than subcutaneous human adipose tissue (AT): Implication of macrophages resident in the AT. *J Clin Endocrinol Metab* 90: 2282–2289.
10. Sartipy P, Loskutoff DJ (2003) Monocyte chemoattractant protein 1 in obesity and insulin resistance. *Proc Natl Acad Sci USA* 100:7265–7270.
11. Ellacott KL, Murphy JG, Marks DL, Cone RD (2007) Obesity-induced inflammation in white adipose tissue is attenuated by loss of melanocortin-3 receptor signaling. *Endocrinology* 148:6186–6194.
12. Nogueiras R, et al. (2007) The central melanocortin system directly controls peripheral lipid metabolism. *J Clin Invest* 117:3475–3488.
13. Butler AA, et al. (2000) A unique metabolic syndrome causes obesity in the melanocortin-3 receptor-deficient mouse. *Endocrinology* 141:3518–3521.
14. Chen AS, et al. (2000) Inactivation of the mouse melanocortin-3 receptor results in increased fat mass and reduced lean body mass. *Nat Genet* 26:97–102.
15. Sutton GM, et al. (2006) Diet-genotype interactions in the development of the obese, insulin-resistant phenotype of C57BL/6J mice lacking melanocortin-3 or -4 receptors. *Endocrinology* 147:2183–2196.
16. Trevaskis JL, et al. (2007) Role of adiponectin and inflammation in insulin resistance of Mc3r and Mc4r knockout mice. *Obesity (Silver Spring)* 15:2664–2672.
17. Ni XP, Pearce D, Butler AA, Cone RD, Humphreys MH (2003) Genetic disruption of gamma-melanocyte-stimulating hormone signaling leads to salt-sensitive hypertension in the mouse. *J Clin Invest* 111:1251–1258.
18. Begriche K, Sutton GM, Fang J, Butler AA (2009) The role of melanocortin neuronal pathways in circadian biology: A new homeostatic output involving melanocortin-3 receptors? *Obes Rev* 10(Suppl 2):14–24.
19. Contreras P, Araya V (1995) [Cushing's syndrome: Review of a national caseload]. *Rev Med Chil* 123:350–362.
20. Dhillo WS, et al. (2003) Agouti-related protein has an inhibitory paracrine role in the rat adrenal gland. *Biochem Biophys Res Commun* 301:102–107.
21. Sainsbury A, et al. (1997) Chronic central neuropeptide Y infusion in normal rats: Status of the hypothalamo-pituitary-adrenal axis, and vagal mediation of hyperinsulinaemia. *Diabetologia* 40:1269–1277.
22. Xiao E, Xia-Zhang L, Vulliémoz NR, Ferin M, Wardlaw SL (2003) Agouti-related protein stimulates the hypothalamic-pituitary-adrenal (HPA) axis and enhances the HPA response to interleukin-1 in the primate. *Endocrinology* 144:1736–1741.
23. Coppola A, et al. (2007) A central thermogenic-like mechanism in feeding regulation: An interplay between arcuate nucleus T3 and UCP2. *Cell Metab* 5:21–33.
24. Björntorp P, Rosmond R (2000) Neuroendocrine abnormalities in visceral obesity. *Int J Obes Relat Metab Disord* 24(Suppl 2):S80–S85.
25. Ahn JD, Dubern B, Lubrano-Berthelier C, Clement K, Karsenty G (2006) Cart overexpression is the only identifiable cause of high bone mass in melanocortin 4 receptor deficiency. *Endocrinology* 147:3196–3202.
26. Farooqi IS, et al. (2000) Dominant and recessive inheritance of morbid obesity associated with melanocortin 4 receptor deficiency. *J Clin Invest* 106:271–279.
27. Klein RF, et al. (2004) Regulation of bone mass in mice by the lipoxygenase gene Alox15. *Science* 303:229–232.
28. Klein RF, et al. (2001) Phenotypic characterization of mice bred for high and low peak bone mass. *J Bone Miner Res* 16:63–71.
29. Zhang Y, et al. (2005) Targeted deletion of melanocortin receptor subtypes 3 and 4, but not CART, alters nutrient partitioning and compromises behavioral and metabolic responses to leptin. *FASEB J* 19:1482–1491.
30. Alon T, et al. (2009) Transgenic mice expressing green fluorescent protein under the control of the corticotropin-releasing hormone promoter. *Endocrinology* 150: 5626–5632.
31. Stanley S, et al. (2010) Identification of neuronal subpopulations that project from hypothalamus to both liver and adipose tissue polysynaptically. *Proc Natl Acad Sci USA* 107:7024–7029.
32. Bowers RR, et al. (2004) Sympathetic innervation of white adipose tissue and its regulation of fat cell number. *Am J Physiol Regul Integr Comp Physiol* 286: R1167–R1175.
33. Shi H, Bartness TJ (2001) Neurochemical phenotype of sympathetic nervous system outflow from brain to white fat. *Brain Res Bull* 54:375–385.
34. Chen HC, Stone SJ, Zhou P, Buhman KK, Farese RV, Jr. (2002) Dissociation of obesity and impaired glucose disposal in mice overexpressing acyl coenzyme a:diacylglycerol acyltransferase 1 in white adipose tissue. *Diabetes* 51:3189–3195.
35. Franckhauser S, et al. (2002) Increased fatty acid re-esterification by PEPCK overexpression in adipose tissue leads to obesity without insulin resistance. *Diabetes* 51:624–630.
36. Haemmerle G, et al. (2006) Defective lipolysis and altered energy metabolism in mice lacking adipose triglyceride lipase. *Science* 312:734–737.
37. Shi H, et al. (2006) TLR4 links innate immunity and fatty acid-induced insulin resistance. *J Clin Invest* 116:3015–3025.
38. Suganami T, et al. (2007) Attenuation of obesity-induced adipose tissue inflammation in C3H/HeJ mice carrying a Toll-like receptor 4 mutation. *Biochem Biophys Res Commun* 354:45–49.
39. Marks DL, Butler AA, Turner R, Brookhart G, Cone RD (2003) Differential role of melanocortin receptor subtypes in cachexia. *Endocrinology* 144:1513–1523.
40. Luquet S, Phillips CT, Palmiter RD (2007) NPY/AgRP neurons are not essential for feeding responses to glucoprivation. *Peptides* 28:214–225.
41. Mountjoy KG, Bird IM, Rainey WE, Cone RD (1994) ACTH induces up-regulation of ACTH receptor mRNA in mouse and human adrenocortical cell lines. *Mol Cell Endocrinol* 99:R17–R20.
42. Penhoat A, Jaillard C, Saez JM (1989) Corticotropin positively regulates its own receptors and cAMP response in cultured bovine adrenal cells. *Proc Natl Acad Sci USA* 86:4978–4981.
43. Bicknell AB, Lomthaisong K, Gladwell RT, Lowry PJ (2000) Agouti related protein in the rat adrenal cortex: Implications for novel autocrine mechanisms modulating the actions of pro-opiomelanocortin peptides. *J Neuroendocrinol* 12: 977–982.
44. Doghman M, et al. (2004) Agouti-related protein antagonizes glucocorticoid production induced through melanocortin 4 receptor activation in bovine adrenal cells: A possible autocrine control. *Endocrinology* 145:541–547.
45. Smart JL, Tolle V, Otero-Corchon V, Low MJ (2007) Central dysregulation of the hypothalamic-pituitary-adrenal axis in neuron-specific proopiomelanocortin-deficient mice. *Endocrinology* 148:647–659.
46. Raff H, Raff JL, Findling JW (1998) Late-night salivary cortisol as a screening test for Cushing's syndrome. *J Clin Endocrinol Metab* 83:2681–2686.
47. Engeland WC, Dallman MF (1975) Compensatory adrenal growth is neurally mediated. *Neuroendocrinology* 19:352–362.
48. Takeda S, et al. (2002) Leptin regulates bone formation via the sympathetic nervous system. *Cell* 111:305–317.
49. Ducy P, et al. (2000) Leptin inhibits bone formation through a hypothalamic relayAa central control of bone mass. *Cell* 100:197–207.

50. Bale L, et al. (2000) Mice deficient for corticotropin-releasing hormone receptor-2 display anxiety-like behavior and are hypersensitive to stress. *Nat Genet* 24:410–414.
51. Segal-Lieberman G, Trombly DJ, Juthani V, Wang X, Maratos-Flier E (2003) NPY ablation in C57BL/6 mice leads to mild obesity and to an impaired refeeding response to fasting. *Am J Physiol Endocrinol Metab* 284:E1131–E1139.
52. Savontaus E, Conwell IM, Wardlaw SL (2002) Effects of adrenalectomy on AGRP, POMC, NPY and CART gene expression in the basal hypothalamus of fed and fasted rats. *Brain Res* 958:130–138.
53. Wardlaw SL, McCarthy KC, Conwell IM (1998) Glucocorticoid regulation of hypothalamic proopiomelanocortin. *Neuroendocrinology* 67:51–57.
54. Schweiger M, et al. (2006) Adipose triglyceride lipase and hormone-sensitive lipase are the major enzymes in adipose tissue triacylglycerol catabolism. *J Biol Chem* 281: 40236–40241.
55. Folch J, Lees M, Sloane Stanley GH (1957) A simple method for the isolation and purification of total lipids from animal tissues. *J Biol Chem* 226:497–509.
56. Abramoff MD, Magelhaes PJ, Ram SJ (2004) Image processing with ImageJ. *Biophotonics International* 11:36–42.